Supplement of

Airborne pollen observations using a multi-wavelength Raman polarization lidar in Finland: characterization of pure pollen types

Xiaoxia Shang et al.

Correspondence to: Xiaoxia Shang (xiaoxia.shang@fmi.fi)
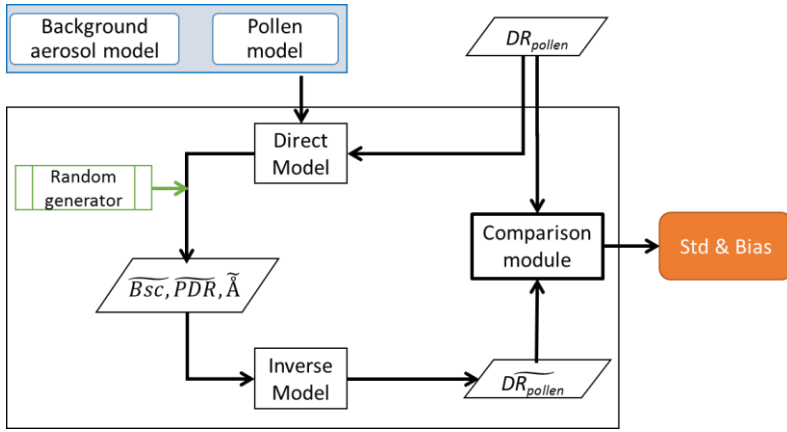
Figure S 1. Block diagram of the end-to-end simulator. Detail description is in section 3.3.
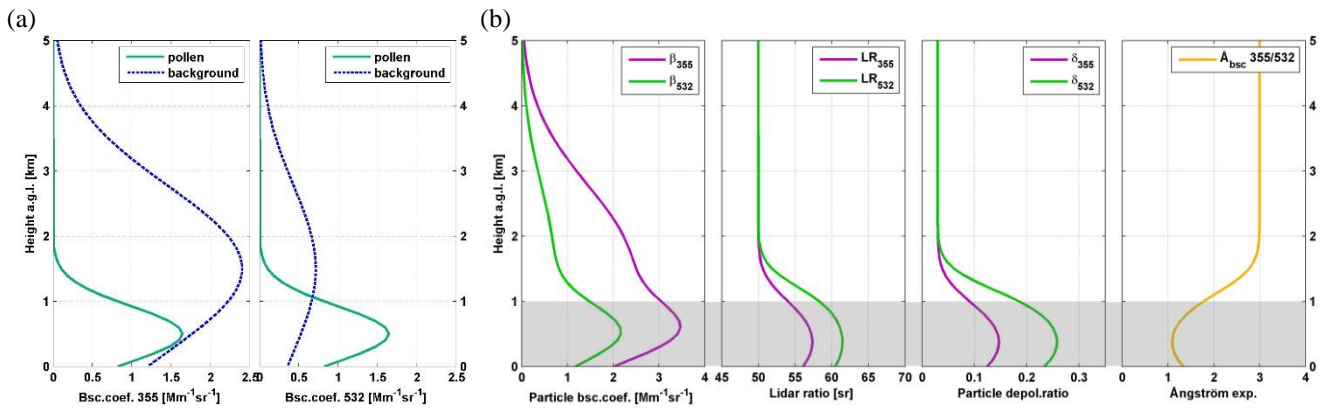
Figure S 2. Simulated profiles from the direct model, using parameters given in Table 3. The values of optical depth of both background and pollen aerosol layers are selected as 0.1 for this case. (a) Simulated backscatter coefficient of pollen (in dark green lines) and background (in dotted blue lines) aerosol layers at 355 nm or 532 nm. (b) Simulated particle backscatter coefficient, lidar ratio, particle depolarization ratio of the total aerosols at 355 nm (in purple) or 532 nm (in green), and backscatter-related Ångström exponent at 355-532 nm. The grey area indicates the defined pollen layer.
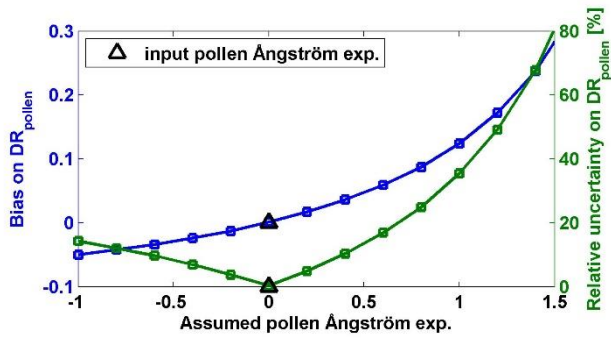
Figure S 3. Examples of estimated bias and relative uncertainty on retrieved pollen depolarization ratio (DR_pollen) against the assumed pollen Ångström exponent. The input pollen Ångström exponent is 0 (shown by black triangles).
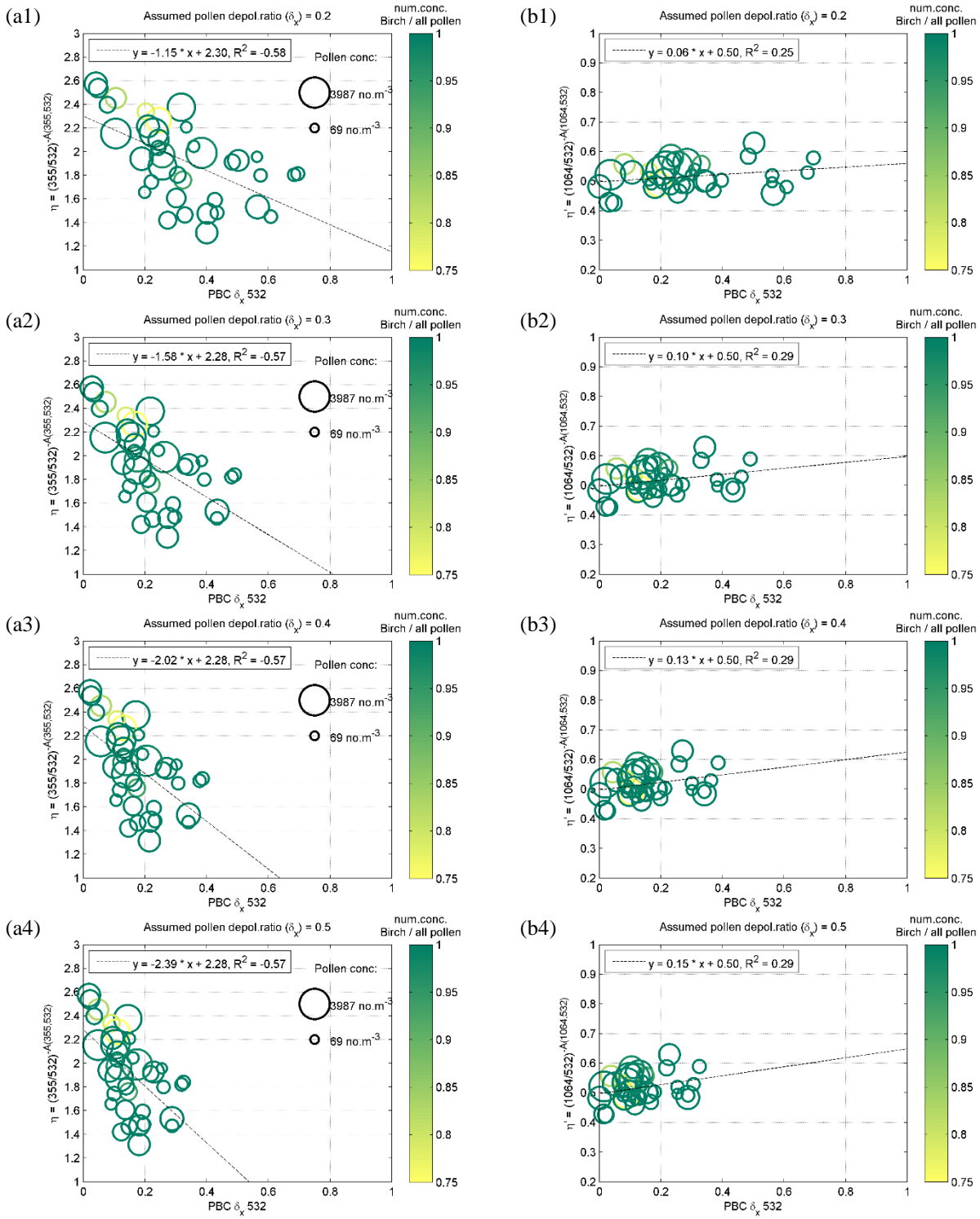
Figure S 4. Similar as Fig. 11 for data during IPP-1. (a1-a4) Mean values of the parameter η (Eq.3, a function of backscatter-related Ångström exponent at 355 -532 nm) against pollen backscatter contribution (PBC) at 532 nm inside the pollen layers. (b1-b4) Mean values of the parameter η' (Eq.8, a function of backscatter-related Ångström exponent at 532 -1064 nm) against pollen backscatter contribution at 532 nm inside the pollen layers. The pollen depolarization ratio at 532 nm (δ_x) is assumed to be 0.2, 0.3, 0.4 or 0.5 (from top to bottom). Linear regression lines are drawn by dotted lines, with fitting equations shown. The correlation coefficient (R^2) is also given. The size denotes the total pollen concentrations measured by the Burkard sampler on roof level; the colour represents the number concentration of the dominant pollen (birch) against the total pollen number concentration.
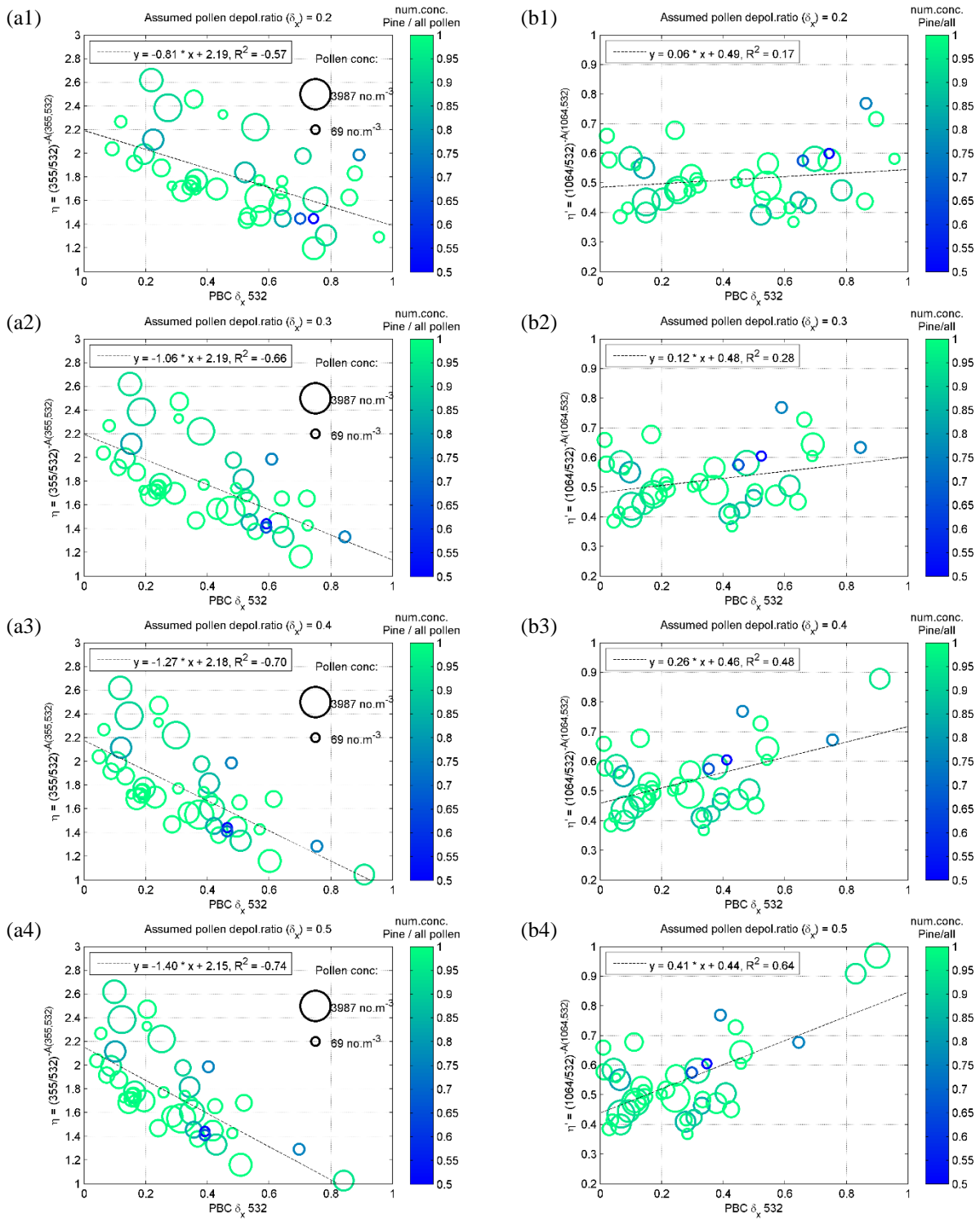
Figure S 5. Same as Fig. S3, but for IPP-3 (pine is dominant pollen).

(a)   (b)
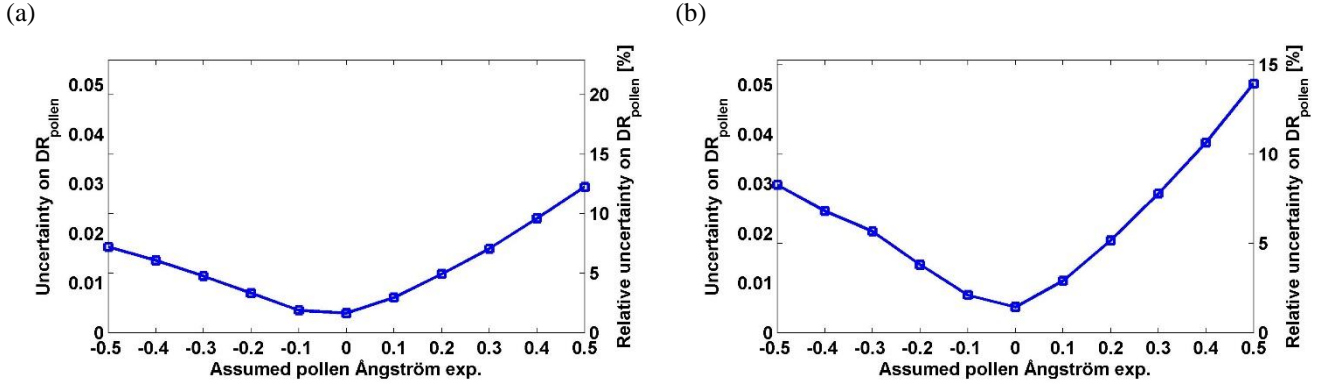
Figure S 6. Estimated uncertainties and relative uncertainties on retrieved pollen depolarization ratio (DR$_{pollen}$) against the assumed pollen Ångström exponent for (a) IPP-1 (birch dominant) and (b) IPP-3 (pine dominant). The initial pollen Ångström exponent was selected as 0. The applied noise level on backscatter coefficients is 10 %. Initial pollen depolarization ratio values were selected as 24 % for birch (a) and 36 % for pine (b). The simulated cases were selected so that the pollen backscatter contribution values range from 2 % to 70 % for birch (a) and 2 % to 90 % for pine (b).
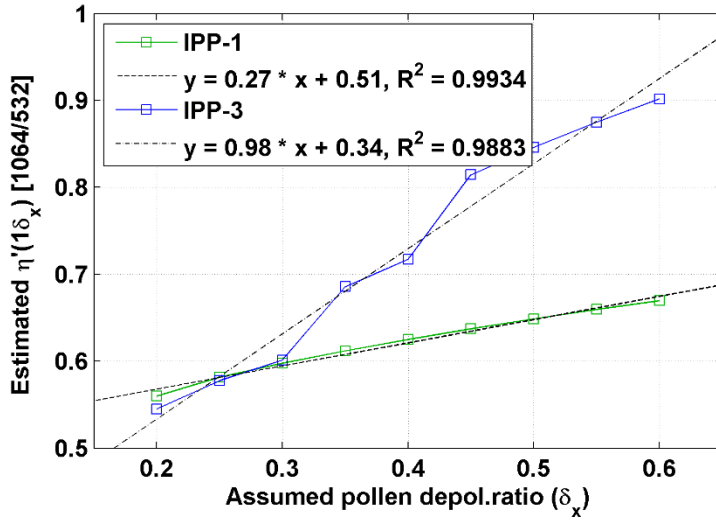
Figure S 7. Similar as Fig. 12, but for the estimated $\hat{\eta}'(1_{\delta_x})$ which is a function of backscatter-related Ångström exponent between 532 and 1064 nm (Eq.8), against the related assumed pollen depolarization ratio δ_x at 532 nm for IPP-1 (in green) and IPP-3 (in blue).
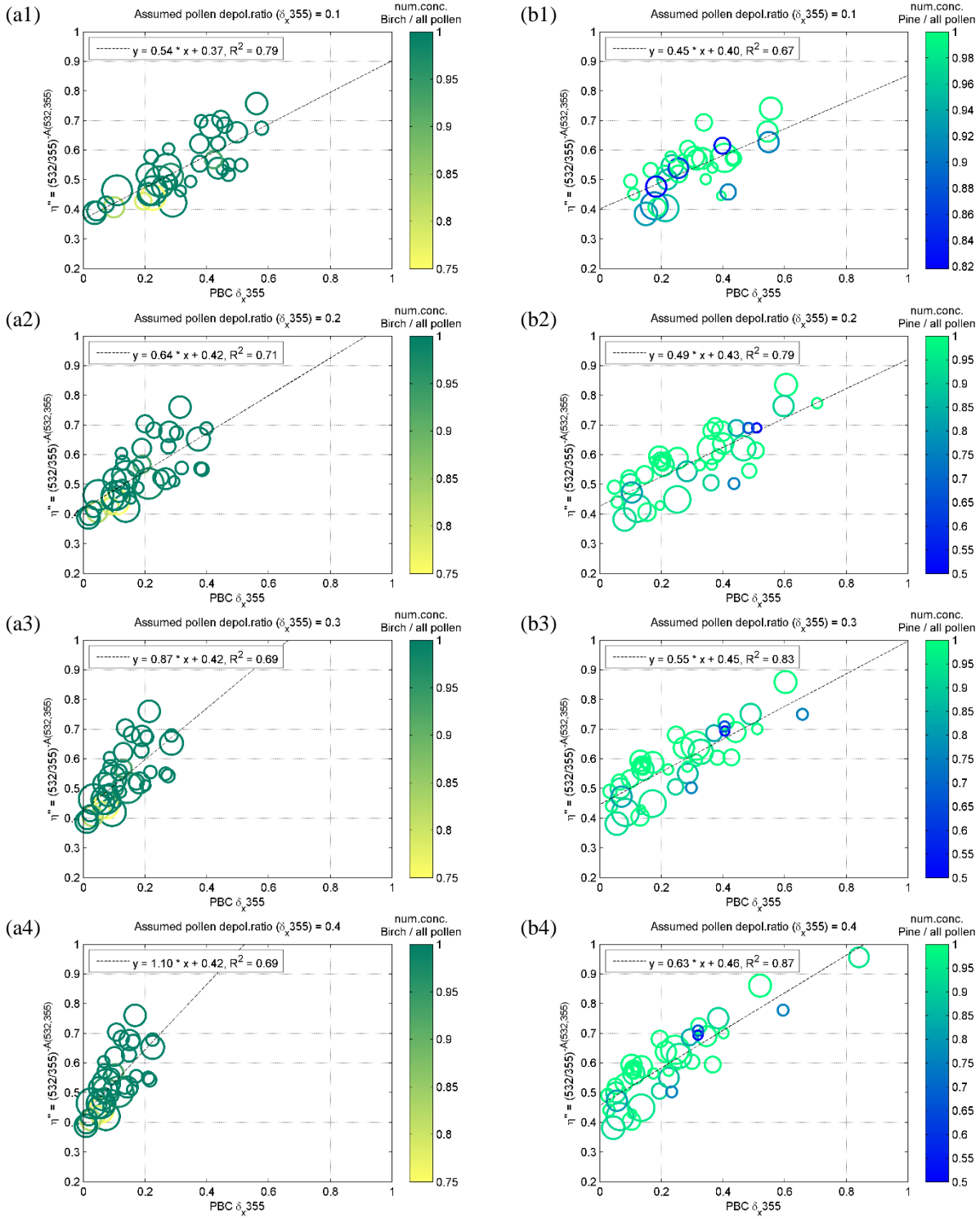
Figure S 8. Similar as Fig. 11 for data during IPP-1 (a1-a4), or IPP-3 (b1-b4), but for mean values of the parameter η'' **(Eq.9, a function of backscatter-related Ångström exponent at 355 -532 nm) against pollen backscatter contribution at 355 nm inside the pollen layers. The pollen depolarization ratio at 355 nm** $(\delta_{x,355})$ **is assumed to be 0.1, 0.2, 0.3, or 0.4 (from top to bottom). Linear regression lines are drawn by dotted lines, with fitting equations shown. The correlation coefficient** (R^2) **is also given. The size denotes the total pollen concentrations measured by the Burkard sampler on roof level; the colour represents the number concentration of the dominant pollen against the total pollen number concentration.**